

Discovery of Red-Skewed K_α iron line in Cyg X-2 with *Suzaku*

Nikolai Shaposhnikov^{1,2}, Lev Titarchuk³ and Philippe Laurent⁴

ABSTRACT

We report on the *Suzaku* observation of neutron star low-mass X-ray binary Cygnus X-2 which reveals a presence of the iron K_α emission line. The line profile shows a significant red wing. This discovery increases the number of neutron star sources where red-skewed iron lines were observed and strongly suggests that this phenomenon is common not only in black holes but also in other types of accreting compact objects. We examine the line profile in terms of models which attribute its production to the relativistic effects due to reflection of X-ray radiation from a cold accretion disk and also as a result of the line formation in the extended wind/outflow configuration. Both models are able to adequately represent the observed line profile. We consider the results of line modeling in the context of subsecond variability. While we were unable to conclusively disqualify one of the models, we find that the wind paradigm has several advantages over the relativistic disk reflection model.

Subject headings: accretion, accretion disks —stars: neutron —X-rays: individual (Cygnus X-2) — stars:

1. Introduction

Recent discoveries of red-skewed iron lines in spectra of neutron star (NS) sources Serpens X-1 (Bhattacharyya & Strohmayer 2007), 4U 1820-30, GX 349+2 (Cackett et al. 2008,

¹ CRESST/NASA GSFC, Astrophysics Science Division, Greenbelt MD 20771; nikolai@milkyway.gsfc.nasa.gov

²University of Maryland, Astronomy Department, College Park, MD 20742

³George Mason University/Center for Earth Observing and Space Research, Fairfax, VA 22030; US Naval Research Laboratory, Code 7655, Washington, DC 20375; email: Lev.Titarchuk@nrl.navy.mil; NASA GSFC, code 661, Greenbelt MD 20771, USA; email:lev@milkyway.gsfc.nasa.gov

⁴CEA/DSM/DAPNIA/SAP, CEA Saclay, 91191 Gif sur Yvette, France;pl Laurent@cea.fr; Laboratoire APC, 10 rue Alice Domont et Leonie Duquet, 75205 Paris Cedex 13, France

C08 hereafter) and 4U 1636-536 (Pandel et al. 2008) show that the phenomenon of red-skewed lines is not restricted to black hole (BH) sources. In this Paper we report on the discovery of the asymmetric iron line in the *Suzaku* spectrum of the NS source Cygnus X-2 (Cyg X-2). Therefore, Cyg X-2 is the fifth NS source which shows strongly asymmetric iron line profile. This indicates that the red-skewed lines in NS sources may be as common as in BH sources. More generally, asymmetric emission lines appear to be abundant in both types of accretion powered X-ray sources. It is crucial to correctly identify the physical origin of the red-skewness of these lines because they can be potentially used to study the properties of the accretion close to accreting objects as well as to constrain the fundamental characteristics of compact objects.

C08 interpreted the K_α iron line profiles in terms of relativistically red-shifted emission due to reflection off the accretion disk very close to a compact object. This scenario is commonly accepted as an explanation of strongly red-skewed iron lines in BH sources (Miller 2007). The main motivation for applying the relativistic line formation scenario to the NS case was the fact that the inner radius of the accretion disk, which was predicted by the relativistic line model was consistent with the interpretation of the highest observed kilohertz quasi-periodic oscillation (kHz QPO) frequency in this sources as a Keplerian frequency at this radius.

A red-skewed profile of emission lines can be also produced by repeated electron scattering in a diverging outflow as proposed by Laurent & Titarchuk (2007), LT07 hereafter, see also references therein. In the framework of the wind model the fluorescent iron line K_α is formed in the partly ionized wind as a result of illumination by central source. Electron scattering of the iron K_α photons within the ionized expanding flow leads to a decrease of their energy (redshift). This photon redshift is an intrinsic property of any outflow for which divergence is positive. Recently Sim et al. (2008) confirmed using multidimensional Monte-Carlo simulation that for sufficiently high wind densities, moderate Fe K_α emission lines can be formed and that electron scattering in the flow may cause these lines to develop extended red wings.

We examine the red-skewed line profile observed in Cyg X-2 both in terms of the relativistic paradigm and in the framework of the wind downscattering. The main obstacle in analyzing the high spectral resolution data with the wind model is that analytical solution is not available for the general formulation of this problem. LT07 used Monte Carlo (MC) simulations to model the line profiles produced in the wind environment. In the presented work we provide a consistent analysis of the line profile with the wind model by introducing the LT07 MC code into XSPEC astrophysical data analysis package. We find that the wind outflow model is able to reproduce the red-skewed line profile with the fit quality similar to

that shown by the relativistic reflection models. Therefore, in order to distinguish between these two models one has to consider their consistency in a broader phenomenological context. For example, C08 proposed to look for high frequency quasi-periodic oscillations (HF QPOs) as an additional evidence of a Keplerian disk existence close to a NS, which then would necessitate the presence of the reflection components in energy spectra. In contrast, the presence of the opaque wind in the system would result in smearing the signal coming from the central region. This smearing effect leads to a suppression of the fast variability of X-ray emission. Unfortunately, high time resolution observations by *Rossi X-ray Timing Explorer (RXTE)*, simultaneous with the *Suzaku* observations analyzed in this Paper, are not available. Thus, we resort to a study based on the *RXTE* data set with similar spectral characteristics. Our comparative analysis indicates that the source was in low variability state during these observations which is more consistent with the wind/outflow scenario.

Description of *Suzaku* and supporting *RXTE* observations as well as details of our spectral fitting are presented in §2. We discuss implications of the relativistic and wind outflow red-skewed line formation scenarios in Cyg X-2 in §3. Conclusions follow in §4.

2. Observations and Spectral Modeling

Cyg X-2 is a low mass X-ray binary (see Lewin et al. 1995, for review) which exhibits a Z-shape color-color diagram (Hasinger & van der Klis 1989). The observations of thermonuclear X-ray bursts (Smale 1998) identified the nature of the compact object in Cyg X-2 as a neutron star. Titarchuk & Shaposhnikov (2002) used the *RXTE* burst data to estimate the NS mass to be about 1.4 solar masses and radius to be about 9 km. Wijnands et al. (1998) reported the simultaneous detection of twin kHz peaks at 500 and 860 Hz and highest single kHz QPO at 1007 Hz.

Cyg X-2 was observed by *Suzaku* (Mitsuda et al. 2007) on May 16, 2006 for a total exposure of 39 ksec (Observation ID: 401049010). However, during more than a half of the observation the satellite were operating in the medium telemetry mode which led to the telemetry saturation and resulted in data unusable for scientific analysis. During intervals when the high telemetry setting were utilized the foreground illuminated XIS detectors (i.e. XIS 0, 2 and 3) operated in 3×3 Event Editing mode with Burst Clock and 1/4 Window settings. The 3×3 Event Editing mode is not available for the XIS 1 for this observation. We therefore used data from XIS 0, 2, and 3 collected when high telemetry rate was utilized. We reduce the *Suzaku* XIS and HXD data using the *xselect* data analysis tool following the

guidelines given by *Suzaku* Data Analysis Guide ¹. The XIS images indicate that strong pile-up in the center of the source point spread function (PSF) leads to a characteristic “crater”. In order to remove piled-up data we extracted XIS spectra from the annulus regions with the outer radius set to the maximum allowed by the XIS detector field of view (~ 115 arcsec) and the inner radius was manually selected to excise the most piled-up inner core of PSF (~ 15 arcsec). The spectra and corresponding responses were extracted by *xselect* extractor and *xisresp*, *xisrmfgen* tools. Spectra and responses for individual detectors were then added using *mathpha* and *addrmf* FTOOLS. We linearly rebin XIS spectral and response data to obtain 1024 spectral channels. HXD/PIN spectrum was corrected for non-X-ray and cosmic X-ray background. We fit XIS and PIN spectra jointly in XSPEC using 0.7-9.0 keV energy range for XIS data and 15.0-40.0 keV range for PIN data fixing the cross-normalization factor between XIS and PIN spectra at unity. Due to large calibration uncertainties we also ignore 1.5-2.5 keV range for XIS spectrum.

For the continuum spectra we choose the sum of thermal (**bbody**) and Comptonized (**comptt**; Titarchuk 1994) components, modified by interstellar photoelectric absorption according to Morrison & McCammon (1983). When we directly fit the data with this model we observe three distinct narrow features in the residuals (See Figure 1, left panel A). First, we see a line signature at 6-7 keV, which is the primary target of our investigation. We also observe a weak excess around 3.2 keV and a prominent line at 1 keV. The feature at 3.2 keV is probably an instrumental artifact. The line at 1 keV was reported previously from Cyg X-2 (Smale et al. 1993) and presumably belongs to the source spectrum. Both features are well represented by **gaussian** shape (see residuals on panel B of Figure 1). In addition to these narrow lines we observe a building-up excess towards higher energies in XIS spectrum. This indicates a presence of a residual pile-up in the regions close to the excised central part of the PSF. To mitigate this effect we utilize the XSPEC **pileup** convolution model designed to model pile-up effect in CCD detectors. The XSPEC implementation of the pile-up model was initially designed to describe this effect in *Chandra* data. However, the model, developed in Davis (2001), is valid for *Suzaku* XIS detectors also. *Suzaku* PSF of XIS CCDs is broader and spreads around larger number of pixels. Therefore, pile-up model for the XIS spectra would require larger number of regions to be considered for pile-up. To model pile-up in XIS detectors we used the following parameter settings for the *pileup* XSPEC model: 2 second time frame, maximum of 10 photons to pile up, unity for grade correction and morphing parameter and 5% of PSF to consider for pile-up. The number of detector regions to consider independently for pile-up was allowed to change which led to the best fit value of 38 regions. This is consistent with the number of 3×3 pixel regions close

¹http://heasarc.gsfc.nasa.gov/docs/suzaku/aehp_data_analysis.html

to excised central core of PSF. This approach successfully removed the hard excess due to the pile-up effect. Finally, we excluded 4.5-7.5 keV energy range where the line emission is expected to be significant and fit the spectrum again to obtain the fit quality of $\chi_{red}^2 = 1.36$. The result is shown in panel D of Fig. 1.

The final best-fit parameters for the continuum model are following: hydrogen column $N_H = 2.3 \pm 0.3 \times 10^{-21} \text{ cm}^{-2}$ for **wabs**; seed photons temperature $T_0 = 0.14 \pm 0.03 \text{ keV}$, electron temperature $kT = 2.27 \pm 0.06 \text{ keV}$, optical depth $\tau_p = 17.3 \pm 0.4$ for **comptt** and **bbody** temperature $T_{bb} = 0.87 \pm 0.01 \text{ keV}$. The energy, sigma and equivalent width (EW) for **gaussians** used to fit lines are $E_L = 1.04 \pm 0.02 \text{ keV}$, $\sigma_L = 0.1 \pm 0.03 \text{ keV}$, $EW = 27.8 \pm 9.0 \text{ eV}$ and $E_L = 3.19 \pm 0.02 \text{ keV}$, $\sigma_L = 0.06 \pm 0.03 \text{ keV}$, $EW = 4.5 \pm 2.0 \text{ eV}$. When we include the iron K_α emission region (4.5-7.5 keV energy band) and fit the spectrum with the relativistic and wind line models the parameter ranges of the above continuum parameters change insignificantly (see Table 1). This indicates that continuum model weakly depends on the assumed line model.

It is worth noting that the values of the continuum parameters imply that during this *Suzaku* observation Cyg X-2 was in the “high/soft” state characterized by high opacity of geometrically thin configuration. Panel E in Fig. 1 shows the residuals of the best-fit model with iron region noticed in the data. The apparent line profile is broad and red-skewed. In fact, the fit with the **gaussian** line model (Model 1) produces the worst fit quality among the applied models $\chi_{red}^2 = 1.34$ (see Table 1).

We apply physically motivated models to describe this red-skewed line profile. Namely, the relativistic models **diskline** (Fabian et al. 1989) and **laor** (Laor 1991) and the wind outflow model **windline** (LT07 MC code). We refer to these models as Model 2, 3 and 4 respectively. The parameters of the **laor** and **diskline** models are: the line energy E_L , inner and outer disk radius R_{in} and R_{out} , emissivity index β_L and inclination angle i_l . During fitting these relativistic models to the data the value of R_{out} was fixed at its default value of $1000 R_G$ and $400 R_G$ for **diskline** and the **laor** respectively. To avoid unphysical results we required the value of the inner radius R_{in} to be greater than $3R_G$ as dictated by the NS compactness limit (see e.g. Lattimer & Prakash 2007). The **windline** model is not a part of the standard set of XSPEC models and is implemented as a local model during our modeling. The **windline** model calculates the line profile by means of MC simulations. The main parameters of the model are the input line energy E_L , the optical depth of the wind τ_w , the wind electron temperature kT_w and the dimensionless wind speed v/c . The additional fixed parameter of the model is the number of individual photons N_{ph} to be used in the MC simulation.

We didn’t observe any significant dependence of the χ^2 -statistic behavior on the number

of photons used in our line simulations for N_{ph} higher than 3×10^3 . For the presented study we used 5×10^3 photons in the `windline` MC simulations. We summarize the results of our modeling and fit quality in Table 1. The resulting values of χ_{red}^2 for Models 2, 3 and 4 are 1.31, 1.30 and 1.32 respectively. In Figure 2 we present the unfolded view of spectral fit with Model 4 where we used 5×10^4 photons in the MC simulation.

We also utilize the data from two *RXTE* observations made on July 25, 2006 and September 4, 2004 (Obs. IDs 92039-01-01-01 and 90030-01-39-00 correspondingly) to investigate the evolution of timing properties of Cyg X-2. We extract the *RXTE*/PCA energy spectra from Standard2 data modes and we use high resolution modes to calculate power density spectra (PDS). We fit *RXTE* energy spectra in XSPEC with the model `wabs(comptt+bbbody+gaussian)`, where `gaussian` is used to model the iron line. N_H column density was fixed at 2.2×10^{21} . We obtain the following best-fit values. For ObsID 92039-01-01-01, `comptt`: $T_0 = 0.001$ keV (unconstrained), $kT_e = 3.06 \pm 0.05$ keV, $\tau_p = 12.6 \pm 0.4$, `bbbody`: $T_{bb} = 1.13 \pm 0.05$ keV, `gaussian`: $E_L = 6.64 \pm 0.17$ keV, $\sigma_L = 0.67 \pm 0.20$ keV, $EW = 86 \pm 25$ eV. For ObsID 90030-01-39-00, `comptt`: $T_0 = 0.16 \pm 0.06$ keV, $kT_e = 2.23 \pm 0.01$ keV, $\tau_p = 14.5 \pm 3$, `bbbody`: $T_{in} = 1.01 \pm 0.02$ keV, `gaussian`: $E_L = 6.57 \pm 0.15$ keV, $\sigma_L = 0.75 \pm 0.15$ keV, $EW = 115 \pm 23$ eV. *Spectral parameters for observation ID 90030-01-39-00 match closely those for the Suzaku spectrum.* All Sky Monitor (ASM) counts rates in 1.5-3/3-5/5-12 keV energy ranges are 14.06/14.85/14.03 cts/s and 13.8/14.07/13.2 cts/s during May 15, 2006 (date of *Suzaku* observation) and during September 4, 2004 (date of 90030-01-39-00 *RXTE* observation) respectively, showing almost the same fluxes and source hardness. This also strongly indicates that during the *Suzaku* observation 401049010 and *RXTE* observation ID 90030-01-39-00 Cyg X-2 was almost in the same state. Thus, we can arguably assume that the timing characteristics of the source during *RXTE* observation 90030-01-39-00 should also be similar to those of the *Suzaku* observation. In Figure 3 we present *RXTE* energy spectra along with the power spectra related to *RXTE* observations 90030-01-39-00 (red), which are expected to be similar to the analyzed *Suzaku* observations, and for the observation 92039-01-01-01 (black).

3. Discussion

The presented evidence for the red-skewed iron line in Cyg X-2 along with the detection of the asymmetric lines in Serp X-1, 4U 1820-30, GX 349+2 (Bhattacharyya & Strohmayer 2007, C08) and 4U 1636-536 (Pandel et al. 2008), increases a number of NS showing this effect to five. This indicates that red-skewed line may be as abundant in NS sources as in BHs (e.g. Miller 2007). C08 interpreted these observed line appearances as the evidence of

relativistic distortion due to the reflection from inner disk located close to the NS surface. The main argument in the association of the line skewness with the inner disk is that the highest observed kilohertz QPO in these sources is consistent with the Keplerian frequency at the inner disk radius predicted by the line profile.

The `diskline` model, when applied to the *Suzaku* (Model 2), leads to the best fit value for the disk inner radius equal to the lower limit set by the model, i.e $6GM/c^2$, which formally translates to the radius of $\simeq 12$ km for the NS mass of $1.4M_{\odot}$. Model 3, which employs the `laor` component to represent the iron line, exhibits the same statistical performance as Model 2 and yields the radius of $9.5 R_G$ or 20 km. We should note that the `laor` model was formulated for the extreme Kerr BH case [see Laor (1991)]. In this model the spin parameter $j = cJ/GM^2$ was assumed to be close to unity. A moderately rotating accreting NS is expected to have a spin parameter less than 0.5. The NS spin in Cyg X-2 is not exactly known but if the difference between kHz QPO of ~ 364 Hz is taken as a spin estimate then the space-time background near Cyg X-2 should satisfy Schwarzschild metric within 10% margin of error.

C08 found that their values of R_{in} were consistent with the inner disk radius predicted by the beat-frequency model (Miller et al. 1998) from kHz QPO values. Maximum kHz QPO value observed in Cyg X-2 is 1007 kHz, which translates to 16.7 km radius if interpreted as a Keplerian frequency at the inner disk. This inferred radius is in between the R_{in} values obtained using `diskline` and `laor` models. Interpretation of the highest kHz QPO peak as a Keplerian frequency is not unique. In the framework of the transition layer (TL) model the *lower* kHz QPO peak is classified as a Keplerian frequency (see Titarchuk 2002, and references therein). The TL model successfully describes the behavior of kHz QPOs in NS sources. The TL model QPO classification leads to the inner disk edge radius of of 22.5 km. Beyond this radius the accreting gas enters the TL to adjust its motion to the rotation of the central star. While the value of the disk inner radius given by the `diskline` model for the iron line can be considered to be in satisfactory agreement with the beat-frequency QPO model, it is harder to reconcile with the TL paradigm.

The red-skewed line - kHz QPO connection is based on the *highest observed* kHz QPO values (C08). However, the duty cycle of kHz QPOs is low. As noted by C08, the most compelling evidence for the inner disk origin of the line would come from the simultaneous observation of the kHz QPOs and the red-skewed iron line. At the time of this writing these two effects were not observed simultaneously from the same source.

The reason for absence of the simultaneous detection of kHz QPOs and broad iron line may be a lack of the correlated observation of high spectral resolution X-ray telescopes (i.e. *Suzaku*/XMM-Newton) and *RXTE*. The Cyg X-2 *Suzaku* observation analyzed in this

Paper is a striking example how this lack of simultaneous coverage creates an obstacle in conducting scientific investigation. Namely, we have to search *RXTE* archive for observation with similar spectral characteristics to estimate timing properties (see the previous section and the discussion below) while simultaneous *RXTE* data would allow directly test timing properties more reliably.

A general idea about the fast timing properties can be inferred based on the archival *RXTE* data by matching the spectral parameters shown by *RXTE* instruments with those observed in the *Suzaku* spectrum in question. This approach is justified by the firmly established correlations between spectral characteristics and timing properties in NS LMXBs (Kaaret et al. 1998) and particularly in Cyg X-2 (Titarchuk et al. 2007). We searched *RXTE* archive for pointing observations nearest to May 16, 2006. Despite the fact that *RXTE* usually conducts frequent monitoring of Cyg X-2, we found that *Suzaku* observation was made in the middle of 140 day gap in *RXTE* monitoring of this source. This, and the fact that Cyg X-2 is changing its state on a daily basis, does not permit us to test subsecond timing variability directly with *RXTE*. Therefore, we have to resort to search for matching spectral properties and rely on spectral-variability correlations. We found that the nearest *RXTE* observation with the spectrum similar to the one shown by *Suzaku* was performed on September 4, 2004 (ObsID 90030-01-39-00, see the previous section). To compare this observation with the spectral state characterized by harder spectrum and lower opacity we arbitrarily choose the observation 92039-01-01-01 which is fit by `comptt` model with parameters $\tau_p = 12.6 \pm 0.4$ and $kT_e = 3.04 \pm 0.02$. In Figure 3 we show the energy and power spectra for these observations. It is clear that the variability for frequencies higher than 0.1 Hz is strongly suppressed and a “forest”-type PDS appears at frequencies above 0.1 Hz. The photon spectrum related to this PDS closely matches the *Suzaku* spectral data. This effect of variability suppression can be readily explained by a smearing of a signal in the opaque wind of optical depth τ_w because the suppression factor is related to the opacity in the wind as $\sim e^{-\tau_w}$. A higher gaussian equivalent width of 115 eV related to 90030-01-39-00 *RXTE* observation with respect to that of 86 eV during 92086-01-01-01 observation is another factor to support the low variability - strong line connection.

The broad band variability continuum observed in PDS can be produced by diffusion of disk small perturbations propagating towards central object. These disk perturbations result in a modulation of inner mass accretion rate, which then leads to variability in the X-ray flux (Lyubarskii 1997). Titarchuk, Shaposhnikov & Arefiev (2007) developed a theory of the diffusive propagation of perturbations in the disk and presented a model for the power spectrum formation. Application of the diffusion theory to the Fourier power spectra of Cyg X-2 and BH source Cyg X-1 led to the conclusion that the fast X-ray variability is produced in two configurations: in a large cold outer accretion disk and a compact geometrically thick

configuration (i.e. transition layer). Long-term variations of the accretion matter supply at the outer accretion disk edge lead to changes of the source spectral state. Specifically, in high-soft state the innermost region becomes very compact and relatively cold as a result of the strong mass accretion. Presumably, this is the state which we are dealing with in the case of *RXTE* observation 90030-01-39-00 and the *Suzaku* observation. However, in this case strong accretion disk presumably extended close to the central object should produce high frequency perturbations leading to a broad band PDS continuum or kHz QPOs in the range ≥ 100 Hz. None of these is seen in our data. This may be attributed to wind/outflow attenuation. It could present a problem for the relativistic disk reflection model of the iron emission line production. We note however, that the origin of fast variability and physical processes governing its evolution are not yet fully understood. Therefore, the above arguments does not provide a solid proof for the wind line model or a dismissal of the relativistic reflection scenario. Futures studies on the asymmetric emission lines in X-ray binaries should address the above points using more substantial observational data. Observation of millisecond variability in the same data which would require wind opacities of 2~3 would provide grounds for the rejection of the wind model. Such cases have not been observed yet. On the other hand, further evidence of the correlation of “forest”-type PDS with the asymmetric line would rule out relativistic reflection paradigm.

Cyg X-2 is a Z source (Hasinger & van der Klis 1989) and presumably accretes at a rate close to the Eddington limit. Therefore, strong outflows are expected in this source, naturally leading to the production of the red-wing of the iron line in this wind/outflow configuration. This hypothesis is supported by the fact that Z sources have strong radio counterparts. Paizis et al. (2006) analysis of radio/X-ray correlation in Z and bright atoll sources that radio and Comptonized emission in these sources originate in same optically thick plasma with the temperature 2.5-3 keV near NS. Moreover, strong requirement for the disk illumination to be concentrated very close to its inner edge (Nandra et al 1999) in the relativistic line formation scenario led Reynolds & Begelman (1997) to consider the production of fluorescent emission within the innermost stable orbit region where matter spirals into the compact object. However, as indicated by the models of Nayakshin et al. (2000) and Ballantyne et al. (2001), the ionization of such a disk by the intense X-ray radiation might further invalidate some of basic assumptions associated with this interpretation. These arguments indicate that the wind/outflow paradigm may indeed be at work as (or at least contribute to) an origin of the red-skewness in the iron lines in compact sources.

4. Conclusions

We present the analysis of the *Suzaku* spectrum from NS Cyg X-2. We discover an K_{α} iron line which shows significant red-wing. This is the fifth NS source so far to show asymmetric line profile. We analyze the line in terms of the relativistic emission from the inner accretion disk and in terms of the wind outflow model.

We conclude that both model are acceptable according to the statistical performance. However, the wind model appears to give more adequate explanation which does not require the accretion disk inner edge to advance close to NS surface. We also consider the line production scenarios in the context of the timing properties. We identify *RXTE* observation which has spectrum very similar to that during *Suzaku* observation which shows the red-skewed line. These *RXTE* data indicate that the source fast variability is strongly suppressed, which can be attributed to smearing in a strong wind. This lack of high frequency variability weakens the red-skewed line connection with kHz QPO and strengthens its connection to a wind/outflow phenomena.

We acknowledge the valuable suggestions by anonymous referee which considerably improved this Paper.

REFERENCES

- Ballantyne, D.R., Ross, R.R. & Fabian, A.C. 2001, MNRAS, 327, 10
- Bhattacharyya, S., & Strohmayer, T. E. 2007, ApJ, 664, L103
- Cackett, E. M., et al.2008, ApJ, 674, 415
- Davis J.E. 2001, ApJ, 562, 575 56
- Fabian, A. C., Rees, M. J., Stella, L., & White, N. E. 1989, MNRAS, 238, 729
- Fabian, A. C. 1995, MNRAS, 277, L11
- Hasinger, G. & van der Klis, M. 1989, A&A, 225, 79
- Kaaret, P., Yu, W., Ford, E. C., & Zhang, S. N. 1998, ApJ, 497, L93
- Laming, J.M. & Titarchuk, L. 2004, ApJ, 615, L121
- Laor, A. 1991, ApJ, 376, 90

- Lattimer, J. M., & Prakash, M. 2007, *Phys. Rep.*, 442, 109
- Laurent, P. & Titarchuk, L. 2007, *ApJ*, 656, 1056
- Lewin, W. H. G., van Paradijs, J., & van den Heuvel, E. P. J. 1995, *Cambridge Astrophysics Series*, Cambridge, MA: Cambridge University Press, —c1995, edited by Lewin, Walter H.G.; Van Paradijs, Jan; Van den Heuvel, Edward P.J.
- Lyubarskii, Yu., E. 1997, *MNRAS*, 292, 679
- Miller, J. M. 2007, *ARA&A*, 45, 441
- Miller, M. C., Lamb, F. K., & Psaltis, D. 1998, *ApJ*, 508, 791
- Mitsuda, K., et al. 2007, *PASJ*, 59, 1
- Morrison, R., & McCammon, D. 1983, *ApJ*, 270, 119
- Nandra, K. et al. 1999, *ApJ*, 523, L17
- Nayakshin, S., Kazanas, D. & Kallman, T.R. 2000, *ApJ*, 537, 833
- Osherovich, V., & Titarchuk, L. 1999, *ApJ*, 522, L113
- Paizis, A., et al. 2006, *A&A*, 459, 187
- Pandel, D., Kaaret, P., & Corbel, S. 2008, *ApJ*, 688, 1288
- Reynolds, C.S. & Begelman, M.C. 1997, *ApJ*, 488, 109
- Sim, S. A., Long, K. S., Miller, L., & Turner, T. J. 2008, *MNRAS*, 388, 611
- Smale, A. P. 1998, *ApJ*, 498, L141
- Smale, A. P., et al. 1993, *ApJ*, 410, 796
- Sobolev, V. V. 1957, *Soviet Astron.*, 1, 678
- Sunyaev, R. A., & Titarchuk, L. G. 1980, *A&A*, 86, 121
- Titarchuk, L. 1994, *ApJ*, 434, 570
- Titarchuk, L. 2002, *ApJ*, 578, L71 .
- Titarchuk, L., & Shaposhnikov, N. 2002, *ApJ*, 570, L25
- Titarchuk, L., Kuznetsov, S., & Shaposhnikov, N. 2007, *ApJ*, 667, 404

Titarchuk, L.G., Osherovich, V.A. & Kuznetsov, S.I. 1999, ApJ, 525, L129

Titarchuk, L., Shaposhnikov, N. & Arefiev, V. 2007, ApJ, 660, 556

Titarchuk, L. & Wood, K. 2002, ApJ, 577, L23

Wijnands, R., et al. 1998, ApJ, 493, L87

Table 1. Best-fit Parameters for the *Suzaku* Spectrum of Cygnus X-2

Parameter	Model 1 ^a	Model 2 ^b	Model 3 ^c	Model 4 ^d
N_H , cm ²	0.23±0.03	0.23±0.03	0.23±0.03	0.23±0.03
T_{bb} , keV	0.87±0.01	0.87±0.01	0.87±0.01	0.87±0.01
T_0 , keV	0.14±0.03	0.14±0.04	0.14±0.03	0.14±0.03
kT_e , keV	2.28±0.02	2.32±0.02	2.35±0.02	2.28±0.02
τ_p	17.2±0.4	17.1±0.4	17.0±0.4	17.2±0.4
E_L , keV	6.65±0.03	6.64±0.14	6.49±0.10	6.78±0.04
σ , keV	0.22±0.04	-	-	-
β_L	-	2.3±0.5	3.0 ^f	-
R_{in}, R_G	-	6.0 ^e	9.5±1.3	-
i_L , deg	-	30.2±6.8	34.0±4.1	-
τ_w	-	-	-	1.29±0.35
v/c , 10 ⁻²	-	-	-	1.43±0.14
kT_w , keV	-	-	-	0.16±0.10
EW_L , eV	28.5±7.1	43.2±11.0	50.6±13.0	37±15
χ^2/N_{dof}	251.2/187	243.3/185	241.4/186	243.5/185

^aXSPEC Model: `wabs(comptt+bbbody+gaussian)`

^bXSPEC Model: `wabs(comptt+bbbody+diskline)`

^cXSPEC Model: `wabs(comptt+bbbody+laor)`

^dXSPEC Model: `wabs(comptt+bbbody+windline)`

^eParameter pegged into the lower boundary value set by the model

^fParameter is fixed. Thawing of the parameter leads to unphysical results.

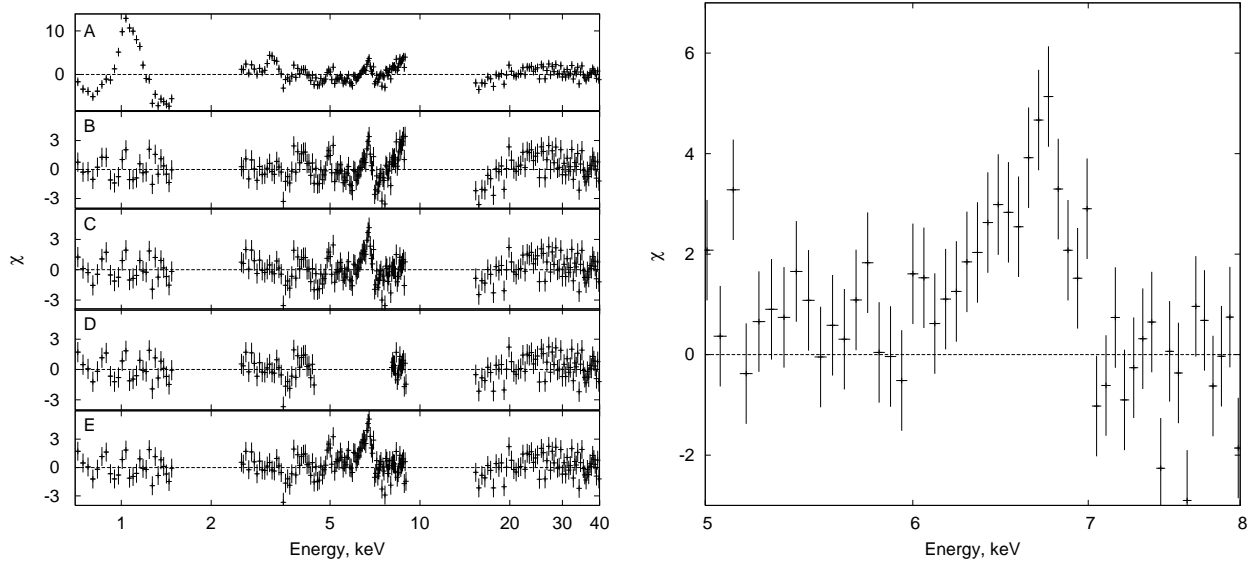


Fig. 1.— *Left panel:* Identification of the continuum model and narrow lines in the *Suzaku* spectrum of Cygnus X-2. Model residuals in units of one sigma error in corresponding channel are shown for A) fit with continuum model `wabs(comptt+bb)` only ($\chi_{red}^2 = 7.5$). B) fit with lines added at 1 keV and 3.2 keV [`wabs(gaussian+gaussian+comptt+bb)`, $\chi_{red}^2 = 2.0$]. C) file up model includes [`pileup*wabs(gaussian+gaussian+comptt+bb)`, $\chi_{red}^2 = 1.7$]. D) fit with energy range from 4.5 keV to 7.5 keV excluded and E) the model obtained in D with channels between 4.5 keV and 7.5 keV noticed. *Right panel:* Panel D on the right side zoomed in the iron line region. Emission line with an apparent red-skewness is seen in the data.

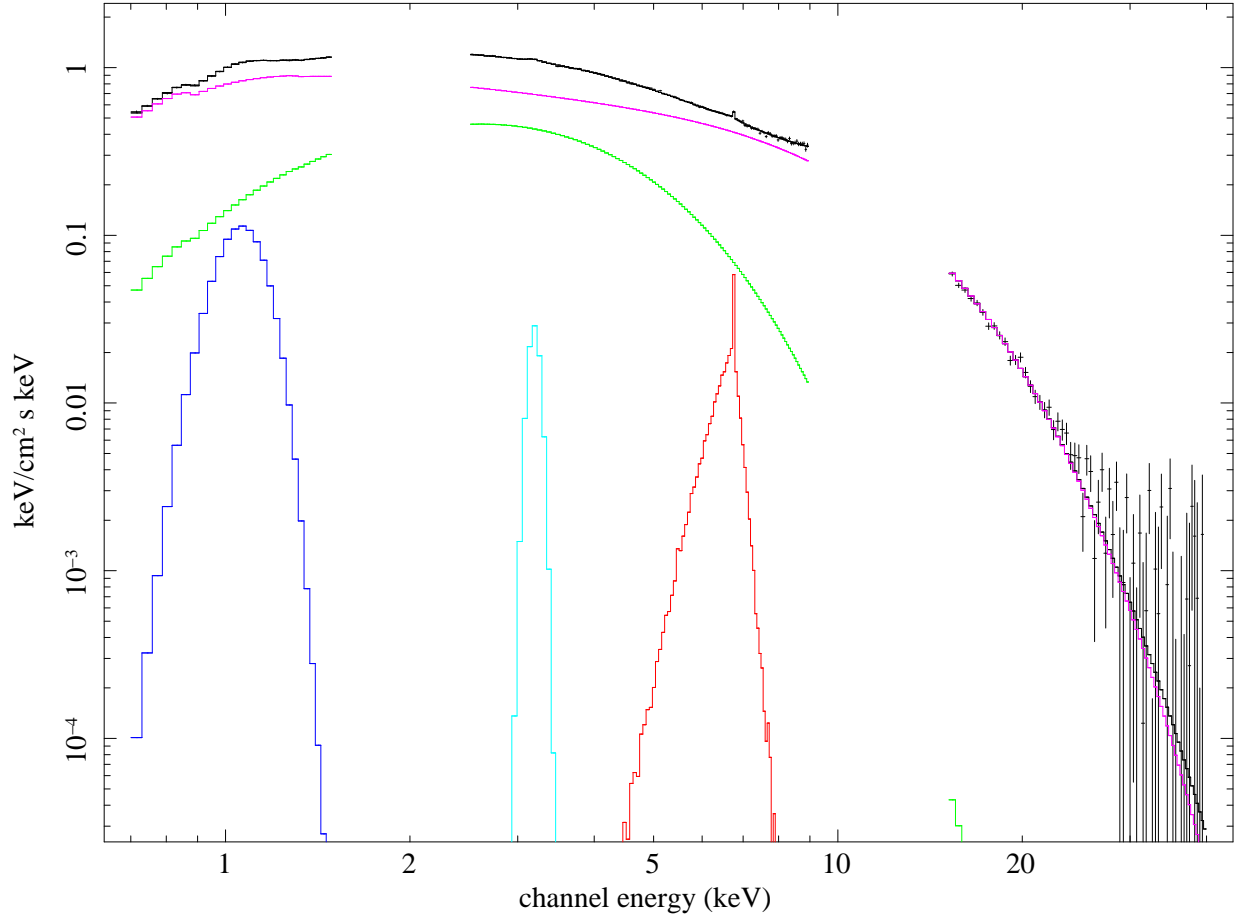


Fig. 2.— Unfolded model fit to the *Suzaku* Cyg X-2 spectrum with the Model 4. The best-fit model of the source spectrum consist of `comptt` (magenta), `bbody` (green), `windline` (red) and two `gaussians` at 1 keV (blue) and 3.2 keV (turquoise).

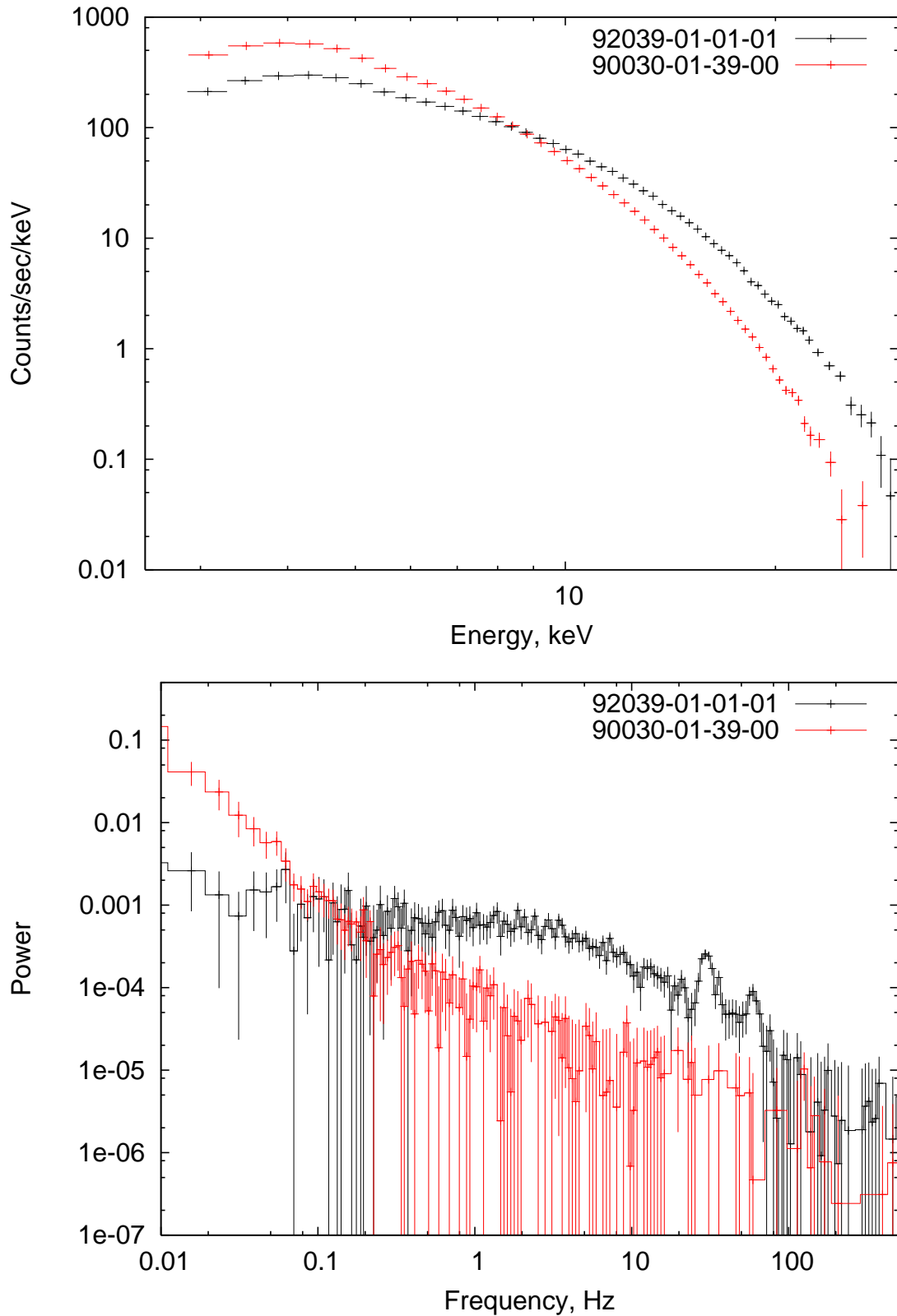


Fig. 3.— Energy and Power Density spectra as observed by *RXTE* during observation 92039-01-01-01 (black) and 90030-01-39-00 (red) . Spectral characteristics for observation 90030-01-39-00 are similar to those measured during *Suzaku* observations. Timing analysis shows that high frequency variability during this observation is strongly suppressed.